Design and Preparation of Highly Filled Water-Borne Polymer–Gibbsite Nanocomposites

*Olessya P. Loiko, Anne B. Spoelstra, Alexander M. van Herk, Jan Meuldijk, and Johan P. A. Heuts**

Highly filled, high solids content, water-borne polymer–Gibbsite nanocomposites are prepared with Gibbsite contents as high as 35 wt%. The polymer–Gibbsite nanocomposites are synthesised via conventional starved feed emulsion polymerization using negatively charged butyl acrylate-*co*-acrylic acid oligomers, which functioned as electrosteric stabilizers for the initial platelets and the subsequently formed latex particles. A simple mathematical model describing the amount of cooligomer required for the colloidal stability of the initial Gibbsite platelets and the subsequently formed particles was derived. This model was used to determine the reaction conditions required for obtaining colloidally stable nanocomposites with a targeted filler content. Cryogenic transmission electron microscopy characterization of the resulting nanocomposites with filler contents up to 20 wt% revealed fully encapsulated Gibbsite platelets and a mixed morphology of "muffin-like" and encapsulated particles was obtained at higher filler contents.

1. Introduction

Polymer–clay nanocomposites have been widely studied over the past decades because of their often superior properties as compared to the unfilled polymer.[1–3] For many properties it is important to control clay arrangement and distribution within the polymer matrix in the final material,[4] and covering every single platelet with a polymer layer is one efficient way of achieving this. Various approaches have been developed to prepare polymer–clay nanocomposites, such as dispersion polymerization,[5] miniemulsion,[6] and emulsion polymerization.[7] Most attempts to encapsulate surface-modified clay platelets, however, resulted in armoured[8] or dumbell-like[9] morphology. Reactions with unmodified platelets have generally led to armoured particles[10] or (partial) coagulation,[11] and until recently, the encapsulation of single platelets remained challenging.

O. P. Loiko, A. B. Spoelstra, Prof. J. Meuldijk, Dr. J. P. A. Heuts
Department of Chemical Engineering and Chemistry
Eindhoven University of Technology
PO Box 513, 5600 MB Eindhoven, The Netherlands
E-mail: j.p.a.heuts@tue.nl
Prof. A. M. van Herk
Institute of Chemical and Engineering Sciences
1 Pesek Road, Jurong Island 627833, Singapore

The discovery of a reversible addition-fragmentation chain transfer (RAFT)-mediated encapsulation method for filler materials,[12] however, caused a significant shift in encapsulation strategy and many examples now exist in which this method was applied successfully.[13–20] We recently extended this method to an atom transfer radical polymerization (ATRP)-based method,[21] which only in the presence of a cross-linker led to encapsulated particles;[22] without cross-linker so-called "muffin-structures" were obtained.[21] Realizing that the charged, reactive, oligomers used in both the RAFT and ATRP approaches in first instance act as stabilizers for the initial clay dispersion and subsequently for the polymer particles, we then used the charged oligomers as unreactive surfactants in a conventional starved-feed emulsion polymerization.[21] This procedure for the encapsulation of unmodified Gibbsite platelets involves the adsorption of (an excess of) anionic cooligomers of butyl acrylate and acrylic acid unto the cationic Gibbsite surface, followed by a conventional starved feed emulsion polymerization and is schematically shown in **Scheme 1**.[23]

A clear effect of cooligomer concentration on the colloidal stability was observed and, as expected, only a limiting amount of polymer per Gibbsite platelet could be stabilized before colloidal instability occurred.[23] The obtained solids content (ϕ_S) in these studies was therefore rather low (i.e., ϕ_S = 17 wt%) and had a very low filler content (ϕ_f) of 0.4 wt%,[23] see Appendix B for the definitions of ϕ_S and ϕ_f. Higher solids and filler contents, however, would be desirable for practical applications.

Polymer–clay nanocomposites with a solids content as high as 50 wt% have been reported in the literature, but most of them were obtained with a relatively low filler content (≤3 wt%);[3,6] only a limited number of publications were dedicated to the preparation of highly filled polymer–clay particles.[3,24,25] These studies indicated that the compounds used for hydrophobization of clay[3,24] and the size of the clay platelets[25] can affect the maximum filler content and that the use of larger amounts of clay platelets may result in less colloidal stability because of an increase in ionic strength of the water phase.[26] It has also been observed that the morphology of the resulting nanocomposites was affected by the filler amount.[24] Overall, it can safely be concluded that the synthesis of highly filled polymer–clay nanocomposites with a controlled morphology still remains a challenge.

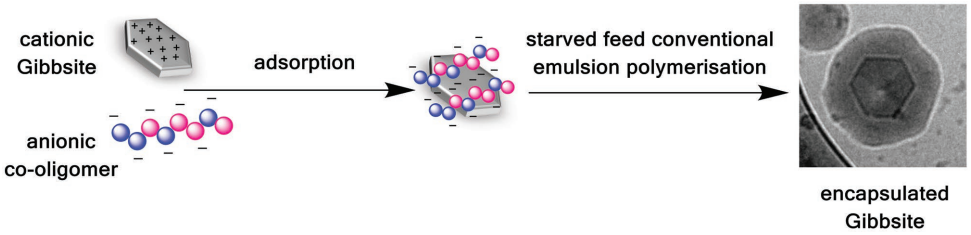

Scheme 1. Representation of the synthesis of polymer–Gibbsite nanocomposites by aqueous starved feed conventional emulsion polymerization using charged cooligomers as stabilizers.

In the current paper, we focus on the synthesis of waterborne spherical polymer–Gibbsite nanocomposites with high solids and filler contents. Using the strategy shown in Scheme 1 we aim at increasing both ϕ_S and ϕ_f in the final product. With the aid of a simple mathematical model we develop an efficient feed strategy with the ultimate aim of increasing ϕ_S from 17 to 40 wt% and ϕ_f from 0.4 to 35 wt%, while maintaining colloidal stability.

2. Results and Discussion

2.1. Method Development

In order to increase the ϕ_S and ϕ_f using our previously reported encapsulation strategy,[23] it is important to realize what limits these parameters in the approach followed thus far. All polymerizations have been carried out using a starved monomer feed to an aqueous dispersion of Gibbsite (G) containing initiator and a fixed amount of anionic cooligomer (S), which was higher than that roughly corresponding to two times the isoelectric concentration (required for a stable Gibbsite dispersion) and lower than that corresponding to the critical micelle concentration (cmc), to avoid secondary nucleation.[27] Within this concentration range of S, it was found that particle growth proceeded in similar ways irrespective of the concentration of S ([S]), but that colloidal instability occurred sooner at lower [S]. Hence, a logical conclusion from this observation is that in order to reach higher polymer contents (per Gibbsite platelet) one needs to feed additional S in such a way that the cmc is not exceeded and the simplest way of doing this is by starting a feed of S just before the colloidal instability occurs. In order to estimate the conditions and time at which feeding of S is required we now derive a simple mathematical model and start by writing the overall mass balance for the cooligomer S. The cooligomer is first used to stabilize the Gibbsite dispersion and provides hydrophobic domains on the platelets that convert the platelets into seed particles (i.e., the number of particles = N_p = initial number of Gibbsite platelets). The amount of S used to stabilize the initial Gibbsite platelets is $n_{S,G}$ and upon particle growth an additional amount of $n_{S,P}$ is required for particle stabilization. We can therefore express the total molar cooligomer amount, $n_{S,T}$ as

$$n_{S,T} = n_{S,G} + n_{S,P} \tag{1}$$

Assuming that the molar amount of cooligomer adsorbed per gram of Gibbsite (m_G) is ϕ, then $n_{S,G} = m_G \times \phi$. The initially nonadsorbed amount of S, $n_{S,P}$, is used to stabilize the formed polymer particle surface and is given by

$$n_{S,P} = N_p \times \frac{A_p}{a_S} \tag{2}$$

where N_p = the number of particles (= number of platelets $\propto m_G$), A_p = the particle surface area, and a_S = the specific area stabilized by one mole of surfactant, i.e., the cooligomer. It should be noted here that the amount of polymer per Gibbsite particle and the overall solids contents are implicitly given by A_p and $N_p \times A_p$, respectively. Equation (1) may now be rewritten as

$$n_{S,T} = m_G \times \phi + N_p \times \frac{A_p}{a_S} \tag{3}$$

From Equation (3), a relatively simple expression for the amount of polymer per gram of Gibbsite for a given cooligomer concentration can now be derived making the following assumptions:

(a) The total number of particles = number of Gibbsite platelets.
(b) Platelet and particle size distributions are monodisperse.
(c) The contribution of the Gibbsite platelet to the resulting polymer–Gibbsite nanocomposite particle is negligible; the particle is treated as a polymer particle.
(d) The amount of surfactant required to stabilize 1 g of platelets is constant and equal to ϕ.
(e) No particle–particle interactions are taken into account.
(f) cmc and a_S are assumed to be independent of the ionic strength.

As can be seen in Appendix A, some straightforward algebra now leads to the following simple equation that relates the amount of polymer per gram of Gibbsite platelet (m_{pol}/m_G) to the used total amounts of cooligomer and Gibbsite

$$\frac{m_{pol}}{m_G} = C \times \left(\frac{n_{S,T}}{m_G} - \varphi\right)^{3/2} \tag{4}$$

where the parameter C is a constant for a given polymer–Gibbsite combination and that contains the polymer density (ρ_{pol}), the number average molar mass of Gibbsite platelets (M_G) and the specific surface stabilized by one mole of the surfactant (a_S)

$$C = \frac{\rho_{pol} \times {M_G}^{1/2} \times {a_S}^{3/2}}{6 \times \pi^{1/2}} \tag{5}$$

Table 1. Recipes and results used for the encapsulation experiments to determine C and ϕ.

	Gibbsite [g]	$n_{S,T}$ [mol]	Polymer[b)] [g]	D_z [nm]	Poly value	ζ [mV]
G-1[a)]	0.20	50.0×10^{-6}	85.0	327	0.13	−24
G-2[a)]	0.20	35.8×10^{-6}	50.0	282	0.11	−20
G-3[a)]	0.20	21.4×10^{-6}	16.0	183	0.14	−25

[a)]Reaction condtions: V_{total} = 0.2 L; MMA:BA = 10:1 w/w; monomer feeding rate = 18 mg min^{-1}; VA-086 = 2 wt% based on monomer; T = 80 °C; [b)]Amount of polymer just before coagulation starts.

Hence, knowledge of the two constants C and ϕ allows for the determination of the maximum amount of monomer per gram of Gibbsite for given total amounts of cooligomer and Gibbsite via Equation (4). Here, we estimated these constants from experiments using previously established reaction conditions,[23] in which we varied $n_{S,T}$ (below the cmc) and monitored the added monomer amount versus time until the coagulation points, i.e., the moment at which coagulation starts (**Table 1**, **Figure 1**).

As expected from our previous paper[23] and as discussed at the beginning of this section (see above), it is clear from Figure 1 that all data points lie on the same straight line, i.e., larger amounts of cooligomer lead to larger amounts of polymer per platelet. Now plotting the data from Table 1 and Figure 1 as m_{pol}/m_G versus $n_{S,T}/m_G$ results in **Figure 2** and nonlinear fitting of these data to Equation (4) yields the following values for the required constants

$$C = 9.2 \times 10^{9} (\text{mol g}^{-1})^{-3/2} \quad \text{and} \quad \varphi = 4.07 \times 10^{-5} \text{ mol g}^{-1}$$

At this point it is thus possible to determine the total amount of cooligomer required to stabilize a certain amount of polymer for a given amount of Gibbsite and to determine what the maximum achievable amount of polymer is for a given cooligomer concentration; the relationships for converting absolute masses of polymer (m_{pol}) and Gibbsite (m_G) into solids (ϕ_S) and filler (ϕ_f) contents and vice versa are given in Appendix B.

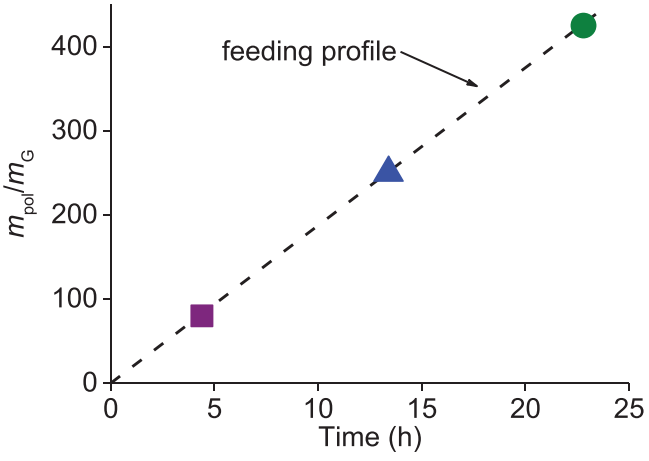

Figure 1. Amount of polymer per Gibbsite platelets as a function of time with recorded coagulation points for constant Gibbsite content (m_G = 0.20 g) and a range of different overall cooligomer amounts: (●) G-1: $n_{S,T} = 50.0 \times 10^{-6}$ mol, (▲) G-2: $n_{S,T} = 35.8 \times 10^{-6}$ mol, and (■) G-3: $n_{S,T} = 21.4 \times 10^{-6}$ mol. Reaction conditions as in Table 1.

Since the aim of this work is to synthesize polymer–Gibbsite nanocomposites with ϕ_S = 40 wt% and $\phi_f \leq$ 35 wt%, we used Equation (4) to calculate the $n_{S,T}$ and from this the $n_{S,P}$ that is required for four different ϕ_f at various ϕ_S (**Figure 3**).

In Figure 3, the maximum allowed amount of free cooligomer (to avoid secondary nucleation) is indicated by a dashed line and only those combinations of ϕ_S and ϕ_f that lie below this line can be achieved without the need for a feed strategy of the cooligomer. For example for ϕ_S = 40 wt% only maximum filler contents of about 5 wt% are possible without feeding of cooligomer or, vice versa, if ϕ_f = 40 wt% is desired, the maximum solids content would be about 25 wt%. If higher solids contents were desired in the latter example, one would need to start feeding additional cooligomer when the amount of monomer added in the semibatch polymerization corresponds to a solids content of about 25 wt%.

Scheme 2 schematically shows the overall strategy for estimating the time at which cooligomer needs to be fed (t_{add}).

For a given volume of water, V_w, the desired solids (ϕ_S) and filler (ϕ_f) contents are trivially converted into absolute masses of polymer (m_{pol}) and Gibbsite (m_G) via the equations shown in Appendix B. Substitution of these values into Equation (4) now leads to the required overall amount of cooligomers ($n_{S,T}$), which is needed to stabilize the initial Gibbsite dispersion and the subsequently formed particles. It is possible that the total amount of cooligomer that is required for particle stabilization ($n_{S,P}$) cannot be added directly at the start of the polymerization as the concentration of free cooligomer needs to remain below cmc to avoid secondary nucleation. Hence the initial amount of

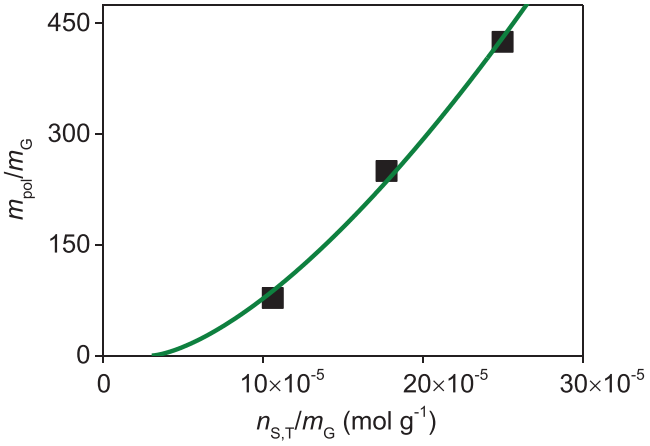

Figure 2. Relation between (m_{pol}/m_G) and ($n_{S,T}/m_G$): (symbols) experimental data and (solid line) nonlinear curve fit using Equation (4). Reaction conditions as in Table 1.

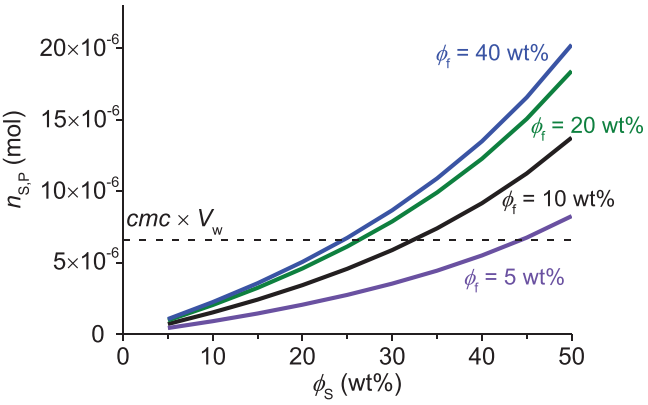

Figure 3. Required $n_{S,P}$ as a function of solid content (ϕ_S) for different filler contents (ϕ_f). V_w = 0.1 L, cmc = 0.067 × 10^{-3} M.

cooligomer, $n_{S,Pinitial}$, may not exceed a value of cmc × V_w and the remainder ($n_{S,Pfeed} = n_{S,P} - cmc \cdot V_w$) needs to be added at a later stage (t_{add}) before colloidal instability occurs, i.e., the conditions at which Equation (4) in combination with $n_{S,T} = m_G \cdot \varphi + cmc \cdot V_w$, $C = 9.2 \times 10^9$ (mol $g^{-1})^{-3/2}$ and $\phi = 4.07 \times 10^{-5}$ mol g^{-1} apply. Equation (4) now leads to the maximum m_{pol}/m_G that can be obtained with this initial charge of cooligomer and the time at which this point is reached (and new cooligomer needs to be added), t_{add}, is now easily determined from the feed rate of the monomer. In principle, one should make sure at this point that the additional amount of cooligomer does not result in a concentration higher than the cmc.

Analogously, but more graphically depicted, the estimation of t_{add} is also possible by addition of a time axis to Figure 3, which indicates the time that a certain solids content is obtained; this time is determined by the monomer feed rate and taking into account that the filler contributes to the overall solids content. The results for the four different situations depicted in Figure 3 are shown in **Figure 4**, and in all four cases t_{add} is easily identified. For instance, to obtain polymer–Gibbsite nanocomposites with ϕ_f = 40 wt% and ϕ_S = 40 wt%, we need to start feeding the remaining cooligomer amount just before t = 19 h during the reaction (Figure 4d).

2.2. Case Studies

Having established a clear experimental strategy, we now use Scheme 2 for designing the experimental conditions for a range of different case studies in which we do not need a cooligomer feed (G-4 and G-5) and in which we do (G-6, G-7, and G-8), depending on the targeted ϕ_S and ϕ_f (**Table 2**). In all cases, we have targeted ϕ_S = 40 wt% and varied ϕ_f from 3 to 35 wt%.

All encapsulation experiments were carried out using the experimental conditions as described in Table 2 and for all these entries the molar mass distributions and conversions were monitored during the polymerization. The particle size distributions and ζ-potentials were measured for the initial and final dispersions. In none of the reactions, loss of colloidal stability was observed and the targeted ϕ_S and ϕ_f were obtained. As an example, only the results of the case with ϕ_S = 40 wt% and ϕ_f = 20 wt% (entry G-7) will be discussed in more detail (**Figure 5**); similar data of the other experiments are presented in the Supporting Information.

The results in Figure 5a clearly demonstrate that the overall monomer conversion follows the monomer feeding rate, indicating truly starved-feed conditions with an instantaneous conversion of 100%. The development of the molar mass distribution during the reaction was followed using size exclusion chromatography (Figure 5b). Bimodal molar mass distributions, in which the cooligomer peak remains constant and a high molar mass peak gradually increases, were observed, which is in accordance with our previous work.[23] These observations are consistent with a conventional emulsion polymerization and a mechanism in which the cooligomer stabilizes the initial Gibbsite platelets and the formed polymer particles. An expected increase in particle size was observed due to polymer formation around the Gibbsite platelets (Figure 5c).

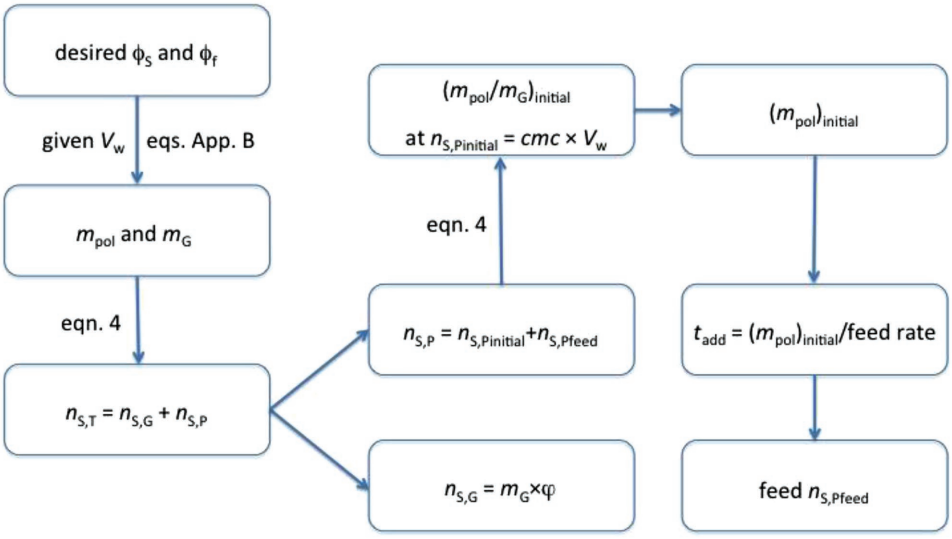

Scheme 2. Sequence of steps toward establishing the necessary reaction conditions.

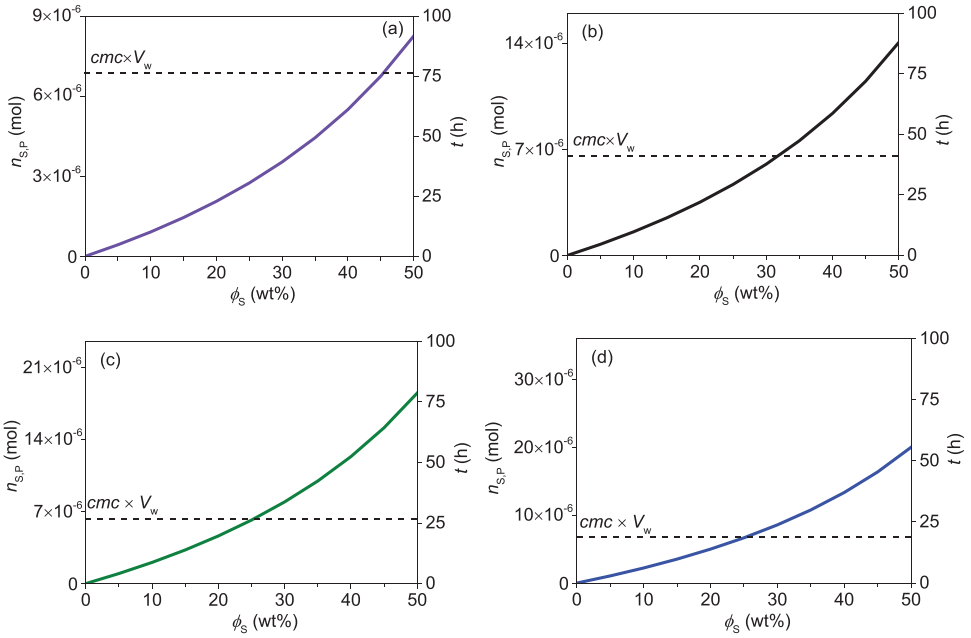

Figure 4. Required feeding time as a function of solid content (ϕ_S) for different filler content (ϕ_f): a) 5 wt%, b) 10 wt%, c) 20 wt%, and d) 40 wt%. Monomer feeding rate = 18 mg min^{-1}. Other conditions as in Figure 3.

Table 3 gives a summary of the characteristics of the final polymer–Gibbsite nanocomposite dispersions. Number-average molar masses (M_n), of the obtained materials range from about 100 × 10^3 to 160 × 10^3 g mol^{-1} with dispersities ($Đ$) ranging from 2 to 3. These values of M_n and $Đ$ are consistent with a conventional emulsion polymerization. The Z-average diameters (D_z) of the final particles determined by dynamic light scattering ranged from about 160 to 260 nm, with relatively low poly values between 0.10 and 0.20. In all cases, the ζ-potential increased from –48 mV to around –20 mV during the process because of an increase in the surface area to be stabilized. These values are in the same range as those of the samples used to determine the parameters C and φ in Equation (4) (i.e., G-1 to G-3, see Table 1), further validating our chosen approach.

Table 2. Experimental design for polymer–Gibbsite nanocomposites synthesis.

	No cooligomer feed		With cooligomer feed		
	G-4	G-5	G-6	G-7	G-8
ϕ_S[a)] [wt%]	40	40	40	40	40
ϕ_f [wt%]	3	7	10	20	35
m_{pol} [g]	35.6	37	39	45	48
m_G [g]	1.1	2.8	4.3	11	26
V_w [mL]	55	60	65	85	110
m_{pol}/m_G	32.3	13.3	9.0	4.0	1.8
$n_{S,T}$[b)] [mol]	4.7×10^{-5}	11.7×10^{-5}	18.0×10^{-5}	46.7×10^{-5}	105.0×10^{-5}
$n_{S,P}$[c)] [mol]	2.5×10^{-6}	3.5×10^{-6}	9.2×10^{-6}	12.8×10^{-6}	14.3×10^{-6}
cmc·V_w[d)] [mol]	3.7×10^{-6}	4.0×10^{-6}	4.3×10^{-6}	5.7×10^{-6}	7.4×10^{-6}
t_{add}[e)] [h]	–	–	33	34	37

[a)]Overall reaction conditions: MMA:BA = 10:1 w/w, VA-086 = 2 wt% based on monomer, T = 80 °C, monomer feeding rate = 18 mg min^{-1}; [b)]Overall required amount of cooligomer determined via Equation (4); [c)]Total amount of cooligomer required for particle stabilization determined via Equation (3); [d)]Maximum value for $n_{S,Pinitial}$ = cmc·V_w, where cmc = 0.067 × 10^{-3} M; [e)]Start of the cooligomer feed determined via procedures shown in Scheme 2, feeding rate = 0.04 mL min^{-1}, $[S]_0 = 10 \times 10^{-3}$ M.

The morphology of the final polymer–Gibbsite nanocomposites was studied using cryogenic transmission electron microscopy. Representative images of all samples are shown in **Figure 6**. It is clear from these images that in experiments with low filler contents up to 10 wt% (Figure 6a–c) every single Gibbsite platelet is completely covered with a polymer layer; the same morphology was reported in our previous work.[23] When increasing the Gibbsite amount (ϕ_f = 20 and 35 wt%), however, encapsulated particles with more than one platelet were observed. Since it is clearly seen from Figure 6d,e that platelets are not stacked, these particles are most likely due to coalesced particles already containing a single platelet. Finally, sample G-8, with ϕ_f = 35 wt%, was the only sample in which two types of morphology were observed (Figure 6e), i.e., the desired particles with the Gibbsite fully encapsulated and the so-called "muffin-like" morphology, which we previously observed in ATRP-mediated nanocomposite formation.[21] Particle counting (>100 particles) showed that about 70% of the particles had the former morphology and about 30% the latter. At this point, we cannot think of any obvious reason for the origin of these "muffin-like" structures.

To summarize we can conclude that with the aid of a simple, but physically sound, mathematical model we were able to design the experimental conditions to successfully obtain stable polymer–Gibbsite nanocomposites with solids contents of 40 wt% and ϕ_f up to 35 wt%.

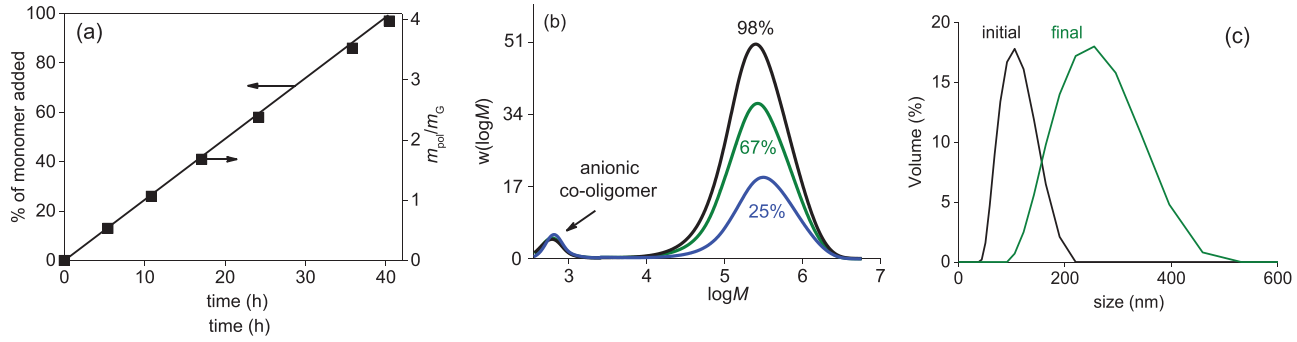

Figure 5. Polymerization characteristics of entry G-7, $\phi_f = 20$ wt% and $\phi_S = 40$ wt%, using the conditions as defined in Table 2. a) Overall monomer conversion expressed as m_{pol}/m_G versus time, b) molar mass distributions, and c) size distribution of polymer–Gibbsite nanocomposites determined via dynamic light scattering.

3. Experimental Section

3.1. Materials

Butyl acrylate (BA, Aldrich, 99%), *tert*-butyl acrylate (tBA, Aldrich, 99%), and methyl methacrylate (MMA, Aldrich, 99%) were passed through a column filled with inhibitor remover before use. CuBr (99.999%, Aldrich), *N,N,N′,N″,N″*-pentamethyldiethylenetriamine (99%, Aldrich), methanol, tetrahydrofuran (THF), trifluoroacetic acid (TFA, 99%, Aldrich), dichloromethane, dimethylformamide, hydrochloric acid (32%, Merck), aluminum isopropoxide (98%, Acros), aluminum sec-butoxide (95%, Fluka), 2,2′-azobis[2-methyl-*N*-(2-hydroxyethyl) propionamide] (VA-086, Wako Chemicals GmbH) were all used as received.

3.2. Characterization

Molar mass distributions, the number-average molar mass (M_n) and dispersity ($Đ$) of the anionic cooligomer and the composite latexes were determined by using size exclusion chromatography (SEC) using a Water SEC equipped with a Waters model 510 pump, a model 410 differential refractometer, and a 2487 dual λ absorbance detector (operated at $\lambda = 254$ nm). A set of two mixed bed columns (Mixed-C, Polymer Laboratories, 30 cm, 40 °C) was used. Tetrahydrofuran was used as the eluent, and the system was calibrated using polystyrene standards (range = 580–7.5 × 10^6 g mol^{-1}). Data analysis was performed using the software Empower Pro version 2 from the Waters Corporation.

^{1}H NMR spectra were recorded on a Varian 400 MHz spectrometer using chloroform-d and water-d2 as solvents. Analysis of the spectra was done using the software MestReNova 9.0.0-12821 from Mestrelab Research S.L.

The particle size distribution and zeta potential (ζ) were determined at 23 °C using a Malvern Zetasizer Nano ZS instrument. The ζ potential was calculated from the electrophoretic mobility (μ) using the Smoluchowski relationship, $\zeta = \eta\mu/\varepsilon$, with ka 1 (where η is the viscosity, ε is the dielectric constant of the medium, k and a are the Debye–Hückel parameter and particle radius, respectively).

Cryo-TEM measurements were conducted on a FEI Cryo-Titan electron microscope operated at 300 kV, equipped with a field emission gun, a post-column Gatan energy filter (GIF), and a post-GIF 2k × 2k Gatan CCD camera. 200 mesh copper grids with lacey carbon layer were used for analysis. The sample vitrification procedure was performed using an automated vitrification robot (FEI Vitrobot Mark III). A 3 µL sample was applied to a Quantifoil grid (R 2/2, Quantifoil Micro Tools GmbH; freshly glow discharged for 40 s just prior to use) within the environmental chamber of the Vitrobot and the excess liquid was blotted away. The thin film thus formed was shot into melting ethane. The grid containing vitrified film was immediately transferred to a cryo-holder (Gatan 626) and observed under low dose conditions at −170 °C.

Table 3. Characterization of polymer–Gibbsite nanocomposites.

	No cooligomer feed		With cooligomer feed		
	G-4	G-5	G-6	G-7	G-8
M_n[a] [g mol^{-1}]	127×10^3	143×10^3	152×10^3	123×10^3	104×10^3
$Đ$[a]	2.9	2.7	2.3	3.0	2.1
D_z[b] [nm]	198	210	172	260	161
poly[b]	0.12	0.13	0.11	0.18	0.16
ζ[b] [mV]	−21	−24	−22	−25	−20

[a]Determined by SEC against PS standards in THF; [b]The initial Gibbsite dispersion had $D_z = 100$ nm, poly = 0.10 and $\zeta = +40$ mV (before cooligomer adsorption) and $\zeta = -48$ mV (after cooligomer adsorption).

3.3. Synthesis of Gibbsite

Gibbsite was synthesized according to the method reported by Wierenga et al.[28] The obtained 1 wt% Gibbsite dispersion was characterized to have a ζ-potential of +40 mV and a Z-average particle diameter (D_z) of 100 nm with a poly value of 0.14 at pH ≈ 7. For the future experiments, we used aqueous dispersions with a different Gibbsite amount (i.e., 10, 20, and 30 wt%).

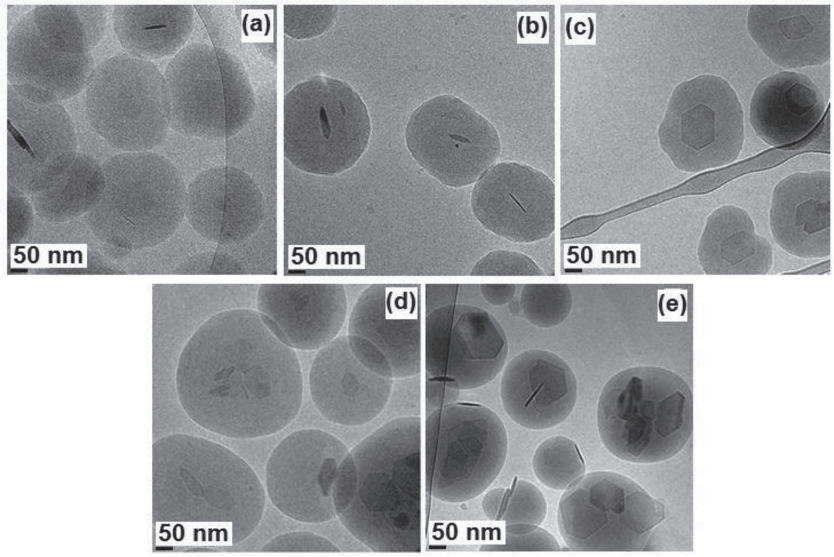

Figure 6. Cryo-TEM images of the final polymer–Gibbsite nanocomposites with different ϕ_f: a) 3 wt%, b) 7 wt%, c) 10 wt%, d) 20 wt%, and e) 35 wt%. Polymerization conditions: as in Table 2.

3.4. Synthesis and Characterization of the Anionic Cooligomers

Butyl acrylate – *tert*-butyl acrylate copolymerization with a monomer composition of 1:2 was carried out under ATRP conditions as previously described.[21] The reaction was performed using [M]:[2-bromo-2-methyl propionic acid phenyl ester]:[*N,N,N′,N″,N″*-pentamethyldiethylenetriamine]:[CuBr] = 200:1:1:1 in 10 vol% dimethylformamide at 70 °C. Final conversion: 10%. ^{1}H NMR (400 MHz, $CDCl_3$, δ): 7.41, 7.25, 7.13 (aromatic H), 4.02 (O—CH_2), 2.22 (—CH_2—CH_2—), 1.82—1.52 (—CH_2—CH_2—C(C=O), 1.45 (O—C(CH_3)$_3$), 0.96 (—CH_3). The cooligomer composition was determined using ^{1}H NMR from the integrated intensity ratios of the area for the aromatic protons (δ = 7.13–7.41) of the end group to the area for the methyl group (δ = 0.96) of butyl acrylate or to the area for *tert*-butyl group (δ = 1.45) of *tert*-butyl acrylate, respectively.[21] Selective hydrolysis of *tert*-butyl acrylate units using TFA was conducted as described previously.[21,29] From the integrations of the proton signals between 0.8 and 2.8 ppm, it was calculated that 97% of the *t*BA was converted into acrylic acid (AA). The resulting cooligomer consisted of four units of butyl acrylate and eight units of acrylic acid with $M_n = 1.4 \times 10^3$ g mol^{-1}, $Đ = 1.15$, and cmc = 0.067×10^{-3} M (measured via dynamic light scattering).[23]

3.5. Adsorption Studies

The adsorption procedure was performed as reported earlier.[21] Particle size distributions and ζ-potentials were measured as described in Section 3.2.[23] The Gibbsite dispersions before monomer addition all had: ζ = –48 mV, D_z = 128 nm (poly = 0.15).

3.6. Encapsulation Experiments

Polymer encapsulated Gibbsite nanoparticles were synthesized by conventional starved-feed emulsion polymerization as described previously.[23]

3.6.1. Experiments without Cooligomer Feeding

Representative example G-4. Briefly, 3.3 mL of a 10×10^{-3} M aqueous stock solution of anionic cooligomer and 39.7 mL of double deionized (DDI) water were transferred into a 250 mL three neck flask after which 12 mL of Gibbsite dispersion (10 wt%) was added drop wise at a rate of 1 mL min^{-1} using a syringe pump NE-1000 under constant stirring at room temperature. The resulting dispersion (pH ≈ 7) was then sonicated for 3 min using a Vibracell tip sonicator at 30% amplitude. 0.68 g of VA-086 initiator (2 wt% based on monomer weight) was added and the reaction mixture was purged with argon for 1 h after which the flask was heated to 80 °C. Finally, 34 g of deoxygenated monomer mixture ([MMA]:[BA] = 10:1 w/w) was fed at a feed rate of 18 mg min^{-1} using a syringe pump NE-1000. After the completion of the monomer addition, the flask was kept stirring at 80 °C for another two hours. During the polymerization, samples were collected to analyze molar mass and particle size distributions.

3.6.2. Experiments with Cooligomer Feeding

Representative example G-7. Briefly, 5.3 mL of a 10×10^{-3} M aqueous stock solution of anionic cooligomer and 24 mL of DDI water were transferred into a 250 mL three neck flask after which 55 mL of Gibbsite dispersion (20 wt%) was added dropwise at a rate of 1 mL min^{-1} using a syringe pump NE-1000 under constant stirring at room temperature. The resulting dispersion was then sonicated for 3 min using a Vibracell tip sonicator at 30% amplitude. 0.9 g of VA-086 initiator (2 wt% based on monomer weight) was added and the reaction mixture was purged with argon for 1 h after which the flask was heated to 80 °C. Then, 45 g of deoxygenated monomer mixture ([MMA]:[BA] = 10:1 w/w) was fed at a feed rate of 18 mg min^{-1} using a syringe pump NE-1000. After 34 h, a fresh amount of cooligomer (0.7 mL of a 10×10^{-3} M aqueous stock solution) was fed using a syringe pump NE-1000 at a feed rate of 0.04 mL min^{-1}. After the completion of monomer addition, the flask was kept stirring at 80 °C for another two hours. During the polymerization, samples were collected to analyze molar mass and particle size distributions.

4. Conclusions

In this paper, we reported a successful operational strategy for the synthesis of highly filled water-borne anisotropic polymer–Gibbsite nanocomposites using a simple mathematical model. The model is based on the amounts of cooligomer that are required for the stabilization of the initial Gibbsite dispersion and for the particles during their subsequent growth

by starved feed emulsion polymerization of MMA/BA. Experimental design using this approach resulted in the desired products with solids contents of 40 wt% and filler contents up to 35 wt%. Cryo-TEM images revealed successful encapsulation of the Gibbsite platelets in the studied cases. However, only in the case of the highest Gibbsite amount of 35 wt% two types of morphology were: encapsulated (70%) and "muffin-like" (30%) hybrid particles.

Appendix A

In this Appendix, Equation (4) is derived. We start with the mass balance for the total required molar amount of cooligomer S ($n_{S,T}$) which is required for stabilizing the initial Gibbsite dispersion ($n_{S,G}$) and the formed particles ($n_{S,P}$)

$$n_{S,T} = n_{S,G} + n_{S,P} \tag{A1}$$

Defining the number of moles of cooligomer adsorbed per gram of Gibbsite as ϕ, the first term on the RHS of Equation (A1) can be written as

$$n_{S,G} = m_G \times \varphi \tag{A2}$$

where m_G is the total mass of Gibbsite particles present.

The second term on the RHS of Equation (A1), $n_{S,P}$, is the amount of cooligomer that is used for stabilizing the formed nanocomposite particles and if the total number of particles is N_p (which is equal to the initial number of Gibbsite platelets), the number of moles of S available per particle, $n_{S,p}$, is given by

$$n_{S,p} = \frac{n_{S,P}}{N_p} \tag{A3}$$

The particle surface area (A_p) that can be stabilized by this amount of S is now determined by the specific area that can be stabilized by one mole of S (a_S) and is given by

$$A_p = n_{S,p} \times a_S \tag{A4}$$

Since the (final) polymer/Gibbsite nanocomposites are spherical[23]

$$A_p = n_{S,p} \times a_S = \pi D^2 \tag{A5}$$

which results in

$$D = \left(\frac{n_{S,p} \times a_S}{\pi} \right)^{1/2} \tag{A6}$$

for the average particle diameter, D, and

$$V_p = \frac{\pi}{6} D^3 = \frac{\pi}{6} \left(\frac{n_{S,p} \times a_S}{\pi} \right)^{3/2} \tag{A7}$$

for the particle volume, V_p.

Ignoring now any contributions of the Gibbsite platelet to the particle volume and mass (which is clearly not the case for very high filler contents!), we can now determine the mass of one particle, $m_{pol,p}$ (stabilized by $n_{S,p}$ moles of cooligomer), from the particle volume and the density of the polymer, ρ_{pol}

$$m_{pol,p} = \rho_{pol} \quad V_p = \rho_{pol} \frac{\pi}{6} \left(\frac{n_{S,p} \times a_S}{\pi} \right)^{3/2} \tag{A8}$$

This equation can now be converted into expressions for the experimentally accessible quantities (m_{pol}/m_G) and ($n_{S,P}/m_G$). Here m_{pol} is the total amount of polymer in the system, thus $m_{pol} = m_{pol,p} \cdot N_p$. Defining M_G as the number average molar mass of the Gibbsite platelet ($M_G \equiv m_G/N_p$), we can express m_{pol}/m_G by

$$\frac{m_{pol}}{m_G} = \frac{m_{pol,p}}{M_G} \tag{A9}$$

The amount of S required to stabilize one particle, can now also be expressed in terms of M_G

$$n_{S,p} = \frac{n_{S,P}}{N_p} = \frac{n_{S,P}}{m_G / M_G} = M_G \left(\frac{n_{S,P}}{m_G} \right) \tag{A10}$$

Substitutions of Equations (A8) and (A10) into (A9) now result in

$$\begin{aligned} \frac{m_{pol}}{m_G} &= \frac{\rho_{pol}}{M_G} \times \frac{\pi}{6} \times \left(\frac{M_G \times n_{S,P} \times a_S}{m_G \times \pi} \right)^{3/2} \\ &= \left(\frac{\rho_{pol} \times M_G^{1/2} \times a_S^{3/2}}{6 \times \pi^{1/2}} \right) \times \left(\frac{n_{S,P}}{m_G} \right)^{3/2} \end{aligned} \tag{A11}$$

In a given system, the parameters ρ_{pol}, M_G, and a_S are constants and Equation (A11) can be simplified to Equation (A12) with a system specific constant C

$$\frac{m_{pol}}{m_G} = C \times \left(\frac{n_{S,P}}{m_G} \right)^{3/2} \tag{A12}$$

Since the total amount of S, $n_{S,T,}$ is experimentally a more useful parameter than $n_{S,P,}$ we use Equations (A1) and (A2) to arrive at

$$\frac{n_{S,P}}{m_G} = \frac{n_{S,T}}{m_G} - \varphi \tag{A13}$$

which, substituted into Equation (A12) results in a simple relationship between (m_{pol}/m_G) and ($n_{S,T}/m_G$)

$$\frac{m_{pol}}{m_G} = C \times \left(\frac{n_{S,T}}{m_G} - \varphi \right)^{3/2} \tag{A14}$$

Appendix B

In this appendix, simple expressions are given to convert the parameters m_{pol} and m_G in Equation (4) and Equation (A14) into overall solids (ϕ_S) ad filler contents (ϕ_f) and vice versa.

The overall solids content in a mixture containing a given mass of water, m_w, is defined as

$$\phi_S = \frac{m_G + m_{pol}}{m_G + m_{pol} + m_w} \quad \text{(B1)}$$

and the filler content (ϕ_f) as

$$\phi_f = \frac{m_G}{m_G + m_{pol}} \quad \text{(B2)}$$

From Equation (B2) follows

$$\frac{m_{pol}}{m_G} = \frac{1-\phi_f}{\phi_f} \quad \text{(B3)}$$

which finally results in the following equation

$$m_G = \frac{\phi_S \times \phi_f}{1-\phi_S} \times m_w \quad \text{(B4)}$$

$$m_{pol} = \left(\frac{1-\phi_f}{1-\phi_S}\right) \times \phi_S \times m_w \quad \text{(B5)}$$

Supporting Information

Supporting Information is available from the Wiley Online Library or from the author.

Acknowledgements

The authors thank the Euro-Asian Cooperation for Excellence and Advancement, Stichting Emulsion Polymerization and the A*STAR Research Attachment Programme for financial support.

Conflict of Interest

The authors declare no conflict of interest.

Keywords

encapsulation, Gibbsite, highly filled nanocomposites

[1] K. Landfester, *Angew. Chem., Int. Ed.* **2009**, *48*, 4488.
[2] M. Micusik, A. Bonnefond, Y. Reyes, A. Bogner, L. Chazeau, C. Plummer, M. Paulis, J. R. Leiza, *Macromol. React. Eng.* **2010**, *4*, 432.
[3] J. Faucheu, C. Gauthier, L. Chazeau, J.-Y. Cavalle, V. Mellon, E. Bourgeat-Lami, *Polymer* **2010**, *51*, 6.
[4] S. S. Ray, *Macromol. Chem. Phys.* **2014**, *215*, 1162.
[5] P. C. Hartmann, N. Greesh, R. D. Sanderson, *Macromol. Mater. Eng.* **2009**, *294*, 787.
[6] Y. Reyes, P. J. Peruzzo, M. Fernandez, M. Paulis, J. R. Leiza, *Langmuir* **2013**, *29*, 9849.
[7] A. M. van Herk, *Macromol. React. Eng.* **2015**, *10*, 22.
[8] T. R. Guimarães, T. C. Chaparro, F. D'Agosto, M. Lansalot, A. M. D. Santos, E. Bourgeat-Lami, *Polym. Chem.* **2014**, *5*, 6611.
[9] D. J. Voorn, W. Ming, A. M. van Herk, *Macromolecules* **2006**, *39*, 4654.
[10] S. Cauvin, P. J. Colver, S. A. F. Bon, *Macromolecules* **2005**, *38*, 7887.
[11] B. zu Putlitz, K. Landfester, H. Fischer, M. Antonietti, *Adv. Mater.* **2001**, *13*, 500.
[12] D. Nguyen, H. S. Zondanos, J. M. Farrugia, A. K. Serelis, C. H. Such, B. S. Hawkett, *Langmuir* **2008**, *24*, 2140.
[13] D. Nguyen, C. Such, B. S. Hawkett, *J. Polym. Sci., Part A: Polym. Chem.* **2012**, *50*, 346.
[14] S. I. Ali, J. P. A. Heuts, B. S. Hawkett, A. M. van Herk, *Langmuir* **2009**, *25*, 10523.
[15] N. Zgheib, J.-L. Putaux, A. Thill, E. Bourgeat-Lami, F. D'Agosto, M. Lansalot, *Polym. Chem.* **2013**, *4*, 607.
[16] V. T. Huynh, D. Nguyen, C. H. Such, B. S. Hawkett, *J. Polym. Sci. Part A: Polym. Chem.* **2015**, *53*, 1413.
[17] D. Nguyen, C. H. Such, B. S. Hawkett, *J. Polym. Sci. Part A: Polym. Chem.* **2013**, *51*, 250.
[18] A. C. Perreira, S. Pearson, D. Kostadinova, F. Leroux, F. D'Agosto, M. Lansalot, E. Bourgeat-Lami, V. Prévot, *Polym. Chem.* **2017**, *8*, 1233.
[19] S. I. Ali, J. P. A. Heuts, A. M. van Herk, *Langmuir* **2010**, *26*, 7848.
[20] S. I. Ali, J. P. A. Heuts, A. M. van Herk, *Soft Matter* **2011**, *7*, 5382.
[21] O. P. Loiko, A. B. Spoelstra, A. M. van Herk, J. Meuldijk, J. P. A. Heuts, *Polym. Chem.* **2016**, *7*, 3383.
[22] O. P. Loiko, A. B. Spoelstra, A. M. van Herk, J. Meuldijk, J. P. A. Heuts, *Polym. Chem.* **2017**, *8*, 2909.
[23] O. P. Loiko, A. B. Spoelstra, A. M. van Herk, J. Meuldijk, J. P. A. Heuts, *RSC Adv.* **2016**, *6*, 80748.
[24] E. Zengeni, P. C. Hartmann, H. Pasch, *Macromol. Chem. Phys.* **2013**, *214*, 62.
[25] Z. Tong, Y. Deng, *Polymer* **2007**, *48*, 4337.
[26] G. Diaconu, M. Paulis, J. R. Leiza, *Polymer* **2008**, *49*, 2444.
[27] W.-D. Hergeth, P. Starre, K. Schmutzler, S. Wartewig, *Polymer* **1988**, *29*, 1323.
[28] A. M. Wierenga, T. A. J. Lenstra, A. P. Philipse, *Colloids Surf., A* **1998**, *134*, 359.
[29] O. Colombani, M. Ruppel, F. Schubert, H. Zettl, D. V. Pergushov, A. H. E. Müller, *Macromolecules* **2007**, *40*, 4338.